



# Reversal of multidrug resistance by co-delivery of paclitaxel and lonidamine using a TPGS and hyaluronic acid dual-functionalized liposome for cancer treatment



Assogba G. Assanhou<sup>a, b, c</sup>, Wenyuan Li<sup>d</sup>, Lei Zhang<sup>a</sup>, Lingjing Xue<sup>a</sup>, Lingyi Kong<sup>a</sup>, Hongbin Sun<sup>a</sup>, Ran Mo<sup>a, \*</sup>, Can Zhang<sup>a, \*\*</sup>

<sup>a</sup> State Key Laboratory of Natural Medicines and Jiangsu Key Laboratory of Drug Discovery for Metabolic Diseases, Center of Drug Discovery, China Pharmaceutical University, Nanjing 210009, China

<sup>b</sup> UFR Pharmacie, Faculté des Sciences de la Santé, Université d'Abomey-Calavi, 01 BP 188 Cotonou, Benin

<sup>c</sup> Jiangsu Key Laboratory of Drug Screening, China Pharmaceutical University, Nanjing 210009, China

<sup>d</sup> Faculty of Pharmacy and Pharmaceutical Sciences, Monash University, Parkville, VIC 3052, Australia

## ARTICLE INFO

### Article history:

Received 30 March 2015

Received in revised form

11 September 2015

Accepted 14 September 2015

Available online 16 September 2015

### Keywords:

Liposome

Paclitaxel

Lonidamine

Combination therapy

Multidrug resistance

## ABSTRACT

Multidrug resistance (MDR) remains the primary issue in cancer therapy, which is characterized by the overexpressed P-glycoprotein (P-gp)-included efflux pump or the upregulated anti-apoptotic proteins. In this study, a D-alpha-tocopheryl poly (ethylene glycol 1000) succinate (TPGS) and hyaluronic acid (HA) dual-functionalized cationic liposome containing a synthetic cationic lipid, 1,5-dioctadecyl-N-histidyl-L-glutamate (HG2C<sub>18</sub>) was developed for co-delivery of a small-molecule chemotherapeutic drug, paclitaxel (PTX) with a chemosensitizing agent, lonidamine (LND) to treat the MDR cancer. It was demonstrated that the HG2C<sub>18</sub> lipid contributes to the endo-lysosomal escape of the liposome following internalization for efficient intracellular delivery. The TPGS component was confirmed able to elevate the intracellular accumulation of PTX by inhibiting the P-gp efflux, and to facilitate the mitochondrial-targeting of the liposome. The intracellularly released LND suppressed the intracellular ATP production by interfering with the mitochondrial function for enhanced P-gp inhibition, and additionally, sensitized the MDR breast cancer (MCF-7/MDR) cells to PTX for promoted induction of apoptosis through a synergistic effect. Functionalized with the outer HA shell, the liposome preferentially accumulated at the tumor site and showed a superior antitumor efficacy in the xenograft MCF-7/MDR tumor mice models. These findings suggest that this dual-functional liposome for co-delivery of a cytotoxic drug and an MDR modulator provides a promising strategy for reversal of MDR in cancer treatment.

© 2015 Elsevier Ltd. All rights reserved.

## 1. Introduction

Chemotherapy is a variant of cancer treatment, which involves the application of one or more types of small-molecule drugs to eradicate the cancer cells, such as alkylating agents, anti-metabolites, anthracyclines and topoisomerase inhibitors. The occurrence of multidrug resistance (MDR) remains the main issue and the major challenge in cancer therapy [1]. MDR can be intrinsic due to inherent physiological factors and acquired with drug resistance factors [2]. Three distinct forms of MDR have been

characterized in detail: 1) classical MDR with an energy-dependent unidirectional membrane-bound drug efflux pump. The efflux pump is composed of a transmembrane glycoprotein (P-glycoprotein, P-gp) encoded by the MDR1 gene [3]; 2) non P-gp MDR that has no P-gp overexpression but displays the same resistance pattern as the classical MDR. The non P-gp MDR is caused by the overexpression of the multi-drug resistance associated protein (MRP) gene [4]; 3) atypical MDR that is associated with quantitative and qualitative alterations in topoisomerase II $\alpha$ , a nuclear enzyme participating in the lethal actions of cytotoxic drugs [2]. Moreover, scientific investigations on the molecular mechanisms of MDR have validated that both classical MDR and non P-gp MDR are related to the activation of the membrane-bound transporter proteins, which depend on to the consumption of ATP and are therefore called ATP-

\* Corresponding author.

\*\* Corresponding author.

E-mail addresses: [rmo@cpu.edu.cn](mailto:rmo@cpu.edu.cn) (R. Mo), [zhangcan@cpu.edu.cn](mailto:zhangcan@cpu.edu.cn) (C. Zhang).

binding cassette (ABC) [5].

Several strategies have been developed to tackle the MDR phenomena. A variety of non-ionic surfactants or polymers that have the inhibiting effect on the P-gp efflux have been applied to overcome classical MDR [6], such as Cremophor EL [7], Tween80 [8], D-alpha-tocopheryl poly (ethylene glycol 1000) succinate (TPGS) [9], Pluronic [10] and chitosan derivatives [11,12]. The inhibition of the overexpressed P-gp can enhance the intracellular accumulation of anticancer drugs that are also P-gp substrates in general, such as paclitaxel (PTX) [13] and doxorubicin [14], which results in enhanced therapeutic efficacies [15]. Alternatively, the reversal of MDR by some specific modulators that can interfere with the intracellular ATP production and the MRP or induce the generation of pro-apoptotic factors has been investigated, such as colchicines [16], 3-bromopyruvate [17], lonidamine (LND) [18]. LND has been demonstrated able to interfere with the mitochondrial function by inhibiting the hexokinase enzyme that is involved in the ATP production, which can also interfere with the respiration and maintenance of the mitochondrial transmembrane potential and prevent aerobic glycolysis in turn [18]. LND with an apoptosis-inducing capacity has been used as a single therapeutic agent [19] or in combination with cytotoxic agents to treat many types of cancer [20,21]. Despite these advances, most of these strategies used alone cannot control and maintain the reversal of the MDR phenomena due to the poor tumor-targeting property of these agents in free forms.

To address this dilemma, nanoparticle-based drug delivery systems (DDSs) have attract more and more attentions for enhanced MDR reversal in cancer therapy [22–26], which can efficiently deliver the therapeutic agents to the tumor tissue by the enhanced permeability and retention (EPR) effect [27] and sequentially to the tumor cells by the typical endocytosis pathway [28]. Liposomes are vesicles made by the dispersion of phospholipids in water [29], which are the most popular delivery system for co-delivery of multiple drugs based on their abilities to encapsulate both hydrophilic and hydrophobic drugs [30]. The TPGS-coated liposomes showed a comparably enhanced circulation behavior with the PEGylated liposomes, thereby increasing the therapeutic efficacy of docetaxel in the breast cancer [31]. Cocktail-based co-delivery of epirubicin-loaded liposomes with LND-loaded liposomes was applied to circumvent the MDR in lung cancer [32], which however suffered from different pharmacokinetic, biodistribution and internalization properties of respective liposomes.

In this study, we developed a TPGS and hyaluronic acid (HA) dual-functionalized cationic liposome (HA-TPGS-CL) for co-delivery of a small-molecule chemotherapeutic drug, PTX with a chemosensitizing agent, LND to treat the MDR cancer (Fig. 1A). The cationic liposome (CL) consists of soybean phosphatidylcholine (SPC), cholesterol (Chol) and a synthetic cationic lipid, 1,5-dioctadecyl-N-histidyl-L-glutamate (HG2C<sub>18</sub>) [33]. TPGS that is anchored in the lipid bilayer of CL serves not only as a P-gp inhibitor to elevate the intracellular drug accumulation [9], but also as a mitochondriotropic substance to endure the liposome with the mitochondrial-targeting capability [34]. HA, the anionic polymer is applied to shield the positive surface charge by electrostatic-driven coating for protection against the blood proteins, which also acts as a tumor-targeting ligand by the specific interaction with the CD44 receptors that is overexpressed in many types of cancer [35]. As illustrated in Fig. 1B, PTX and LND co-loaded HA-TPGS-L (designated as PTX&LND-HA) after intravenous injection preferentially accumulates at the tumor site by the passive and active tumor targeting effects as expected, followed by the CD44-mediated internalization and transport into the endocytic vesicles, endosomes and lysosomes. Hyaluronidase (HAase) that is rich in the tumor extracellular matrix and endo-lysosomes [36] degrades the

HA shell of PTX&LND-HA and allows the exposure of the TPGS-modified CL. In the endo-lysosomes, the high cationic property of CL combined with the proton sponge effect of the imidazole groups of histidine in CL facilitates endo-lysosomal escape and cytoplasmic distribution of the liposome [37–39]. TPGS inhibits the P-gp efflux of the released PTX or LND to maintain high therapeutic concentrations of drugs within the cancer cells, and also helps the liposome target the mitochondria. The released LND interferes with the mitochondrial function and thereby suppresses the intracellular production of ATP that is an energy source of P-gp [18], which further results in enhanced P-gp inhibition. Furthermore, LND is able to sensitize the cancer cells to PTX [40,41], which can also induce the cell apoptosis in combination with PTX to efficiently eliminate the MDR cancer cells.

## 2. Materials and methods

### 2.1. Materials

PTX was purchased from Yew Pharmaceutical Co. Ltd. (Jiangsu, China). LND was purchased from Chang Zhou Rui Ming Pharmaceutical Co. Ltd. SPC (LIPOID S 100) was acquired from Shanghai Wandong Biologic technological Co. Ltd. Chol was provided by Huixing Biochemical Reagent Co. Ltd. (Shanghai, China). TPGS was purchased from SPERIZOL Pharma (DUSSELDORF). HA was purchased from Zhenjiang Dong Yuan Biotech Co. Ltd. (Jiangsu, China). HAase, sucrose, amiloride and nystatin were purchased from Sigma Aldrich. Rhodamine 123 (RH123) and Mitochondria Isolation Kit were bought from the Beyotime Institute of Biotechnology (Nantong, China). Dulbecco's modified eagle's medium (DMEM), RPMI 1640 medium and trypsin (Gibco®) were purchased from Pufei Biotechnology Co. Ltd. (Shanghai, China). Fetal bovine serum (FBS, Hyclone®), penicillin-streptomycin solution (Hyclone®), phosphate buffered saline (PBS, Hyclone®) and 3-(4,5-dimethylthiazol-2-yl)-2,5-diphenyltetrazolium bromide (MTT) were provided by Sunshine Biotechnology Co. Ltd. (Nanjing, China). BCA protein assay kit was purchased from Thermo Scientific. 1,1'-Diocetadecyl-3,3',3'-tetramethylindotricarbocyanine iodide (DiR) was purchased from Life Technologies.

### 2.2. Preparation and characterization of liposome

The cationic lipid, HG2C<sub>18</sub> was synthesized as described previously [33]. Cationic liposome (CL) was prepared using the lipid film hydration method [42]. PTX, LND, SPC, HG2C<sub>18</sub> and Chol were weighed at the ratio of PTX:LND:lipid = 1:4:50 (w:w:w) and SPC:HG2C<sub>18</sub>:Chol = 27:9:4 (w:w:w) and dissolved in the mixture of chloroform:methanol (2:1, v:v). The organic solvent was then evaporated using the rotary evaporator at 40 °C to form the lipid film. The solvent was totally evaporated under vacuum overnight. The lipid film was rehydrated with the purified water, and followed by homogenization with the rotary evaporator at 37 °C at low speed, to allow the formation of the multilamellar vesicle (MLV). The small unilamellar vesicles (SUV) were formed from the MLV by ultrasonication. The drug-loaded CL (PTX&LND-CL) was obtained after successive filtration through 0.8, 0.45 and 0.22 μm membrane filters. For preparation of TPGS-functionalized liposome (TPGS-L), TPGS at the ratio of TPGS:lipid = 9:20 (w:w) was added into the components and dissolved in the mixture of chloroform:methanol (2:1, v:v). The following preparation method was similar to that of CL. The HA-coated and TPGS-functionalized drug-loaded liposome (PTX&LND-HA) was obtained by adding PTX&LND-TPGS-L into the HA solution at the ratio of HA:lipid = 1:20 (w:w) and incubating under stirring overnight. For preparation of RH123-loaded or DiR-labeled liposome, RH123 at the ratio of RH123:lipid = 1:1053



and centrifuged at 14,000 g for 10 min. The amounts of PTX and LND released were determined using HPLC.

### 2.5. Degradation of HA

The HAase-mediated degradation of HA was evaluated by monitoring the change in particle size and surface charge of HA-coated liposomes after treatment with HAase. The mixture of HA-coated liposome and HAase (1 mg/mL) (1:1, v:v) was placed in the 37 °C water bath at pH 4.5 and pH 7.4 under shaking. At a predetermined time, the samples were withdrawn. The particle size and zeta potential were measured.

### 2.6. Cell culture

Human breast adenocarcinoma (MCF-7) cells, multidrug resistant MCF-7 (MCF-7/MDR) cells and human lung carcinoma (A549) cells were obtained from the Cell Bank of Chinese Academy of Sciences (Shanghai, China). The culture conditions were listed as follows: MCF-7 cells: DMEM with 10% (v:v) FBS; MCF-7/MDR cells: 1640 medium with 15% (v:v) FBS; A549 cells: 1640 medium with 10% (v:v) FBS. All the medium was supplemented with 100 U/mL penicillin and 100 µg/mL streptomycin. The cells were cultured in an incubator at 37 °C under an atmosphere of 5% CO<sub>2</sub>.

### 2.7. Cellular uptake and endocytosis pathway

MCF-7/MDR cells at a density of  $1 \times 10^5$  cell/well were seeded and cultured in 24-well plates for 48 h. The cells were incubated with different drug-loaded liposomes for different time at 37 °C. After incubation, the cells were washed twice with cold PBS. 160 µL of cell lysis buffer (Beyotime, China) was added and incubated for 30 min. The BCA protein assay kit (Thermo Scientific) was used for quantifying the protein amount, while the drug concentration was determined using HPLC. The cellular uptake ( $Q_{\text{drug}}/Q_{\text{protein}}$ ) was calculated, where  $Q_{\text{drug}}$  and  $Q_{\text{protein}}$  are the quantities of drug in the cells and cell protein, respectively.

To investigate the active targeting effect of the HA shell on the liposomes, the competitive inhibition study was first applied. The cells, including CD44-overexpressing MCF/MDR cells [43] and A549 cells [44] and CD44-deficient MCF-7 cells [45], were incubated with the free HA (10 mg/mL) for 1 h at 37 °C, followed by incubation with the HA-coated liposome (5 µg/mL PTX) for 4 h at 37 °C. Furthermore, the HA-coated liposome was pre-treated with HAase (1 mg/mL) for 1 h at pH 4.5, and MCF-7/MDR cells were then incubated with the HAase-treated HA-coated liposome for 4 h at 37 °C. The cells were treated following the same procedure as described above, and the cellular uptake was determined and compared under different conditions.

The endocytosis pathway of the liposomes was determined. MCF-7/MDR cells at a density of  $1 \times 10^5$  cell/well were seeded and cultured in 24-well plates for 48 h. After incubation with the specific endocytosis inhibitors [sucrose (154 mg/mL) for clathrin-mediated endocytosis inhibition, nystatin (15 µg/mL) for caveolin-mediated endocytosis inhibition, and amiloride (133 µg/mL) for macropinocytosis inhibition] for 1 h at 37 °C [42], the cells were incubated with different liposome preparations containing 5 µg/mL PTX for 4 h. The same procedure was followed as described in the cellular uptake study above. The cellular uptake was determined, and the relative uptake efficiency was calculated under different conditions.

### 2.8. Enhanced intracellular accumulation by inhibiting P-gp efflux

To demonstrate the effect of the functionalized liposome on

inhibiting the P-gp efflux for increased intracellular accumulation, we investigated the influence of TPGS or TPGS-containing liposomes on the cellular uptake of RH123. MCF-7/MDR and MCF-7 cells at a density of  $1 \times 10^5$  cell/well were seeded in 24-well plates, and cultured for 48 h. The cells were incubated with the free RH123 (5 µM) in the presence of different concentrations of TPGS for different time, followed by observation using fluorescence microscope (Olympus, Japan). Moreover, MCF-7/MDR cells were incubated with the free RH123 (5 µM) in the presence of different TPGS formulations for 1 h. The cells were then washed twice with cold PBS and collected, followed by centrifugation at 600 g for 5 min and washing twice with cold PBS. The fluorescence intensity of RH123 in the cells was determined using flow cytometry. In addition, MCF-7/MDR cells were further incubated with different RH123-loaded liposomes (5 µM) for 1 h. The fluorescence intensity of RH123 in the cells was determined using flow cytometry.

### 2.9. Intracellular delivery

The intracellular delivery of the liposome in MCF-7/MDR cells such as endo-lysosomal escape and mitochondria targeting was monitored using confocal laser scanning microscope (CLSM). MCF-7/MDR cells at a density of  $1 \times 10^5$  cell/well were seeded in a CLSM dish (NEST). After 24 h of culture, the cells were incubated with different RH123-loaded liposomes (5 µM RH123) at 37 °C for 3 and 6 h. The late endosome and lysosome were stained with Lyso-Tracker Red (50 nM) at 37 °C for 0.5 h. On the other hand, the cells were incubated with different RH123-loaded liposomes (5 µM RH123) for 12 h. The mitochondria were stained with MitoTracker Red (200 nM) at 37 °C for 0.5 h. After staining, the cells were washed with cold PBS twice and immediately observed using CLSM (Leica, Germany).

The content of RH123 in the mitochondrial fraction was quantified using flow cytometry [42,46]. MCF-7/MDR cells at a density of  $1 \times 10^5$  cell/well were cultured in 6-well plates for 48 h at 37 °C, and incubated with different RH123-loaded liposomes (5 µM RH123) for 12 h. The cells were washed with cold PBS twice and then trypsinized. After stopping the trypsinization by adding cold complete medium, the cells were centrifuged at 600 g for 5 min and washed twice with cold PBS. The isolation of mitochondria was performed according to the protocol of mitochondria isolation kit (Beyotime, China). Subsequently, the cells were resuspended in the mitochondria isolation buffer and subjected to 15 strokes in a Dounce homogenizer to obtain a cell homogenate. The solution was then centrifuged at 600 g for 10 min. The supernatant was then centrifuged at 11,000 g for 10 min to pellet mitochondria. The pelleted mitochondrial fraction was resuspended in mitochondria stock buffer and immediately analyzed using flow cytometry (Becton Dickinson, USA).

### 2.10. Inhibition of intracellular ATP production

The intracellular ATP levels were measured using an ATP assay kit (Beyotime, China) after MCF-7/MDR cells were treated with different formulations. MCF-7/MDR cells at a density of  $1 \times 10^5$  cell/well were seeded and cultured in 12-well plates for 24 h, and were then incubated with different drug-loaded liposomes (12.5 µg/mL PTX and/or 50 µg/mL LND) for 8 h at 37 °C. The content of ATP in the cells was determined by following the manufacturer's protocol. Briefly, the cell suspension was obtained by using cell lysate provide by the kit, followed by centrifugation at 12,000 g for 5 min at 4 °C. 100 µL of the supernatant was mixed with 100 µL of ATP detection working dilution on a black 96-well plate and keep for 10 min. The luminescence intensity was measured using a microplate reader (Luminoskan ascent, Thermo Scientific).

### 2.11. Cell apoptosis

The effect of different drug-loaded liposomes on cell apoptosis was first evaluated using the Hoechst and propidium iodide (PI) double staining method [47]. MCF-7/MDR at a density of  $1 \times 10^5$  cell/well were seeded and cultured in 6-well plates for 48 h at 37 °C, and were then incubated with different drug-loaded liposomes (12.5 µg/mL PTX and/or 50 µg/mL LND) for 12 h. The cells were washed twice with cold PBS and stained with the mixture of Hoechst 33258 (5 µg/mL) and PI (10 µg/mL) for 10 min. After washing with cold PBS, the cells were observed using the fluorescence microscope.

The apoptosis-inducing capability of different drug-loaded liposomes was also assessed using the Annexin V-FITC/PI apoptosis detection kit (Vazyme Biotech, China). MCF-7/MDR cells at a density of  $1 \times 10^5$  cell/well were seeded and cultured in 6-well plates for 48 h at 37 °C, and were then incubated with different drug-loaded liposomes (12.5 µg/mL PTX and/or 50 µg/mL LND) for 12 h. The following process was in accordance to the manufacturer's protocol. The treated cells were analyzed using the flow cytometry.

### 2.12. In vitro cytotoxicity

The MTT assay was used to examine the in vitro cytotoxicity of different drug-loaded liposomes and blank liposomes against MCF-7/MDR cells. The cells at a density of  $5 \times 10^3$  cell/well were seeded and cultured in 96-well plates for 24 h at 37 °C, and were then incubated with different drug-loaded liposomes or blank liposomes for 48 h. Afterward, 20 µL of MTT (5 mg/mL) was added to each well and incubated again for 4 h. The solution was then removed and 150 µL of DMSO was added to each well. The absorbance was measured at a test wavelength of 570 nm and a reference wavelength of 630 nm by the microplate reader. The cell viability was calculated.

### 2.13. Animals and xenograft tumor models

Sprague–Dawley (SD) rats (male, 180–220 g) and BALB/c nude mice (female, 18–25 g) were purchased from the College of Veterinary Medicine at Yangzhou University (Jiangsu, China). The animal experiments were performed in compliance with the Guide for Care and Use of Laboratory Animals, approved by China Pharmaceutical University. To establish xenograft tumor models, MCF-7/MDR cells at a density of  $2 \times 10^7$  cell/mouse were subcutaneously injected into the upper back area of the nude mice. Tumor progression was monitored by the caliper measurements of tumors along the length and width. Tumor volumes ( $L \times W^2/2$ ) were calculated, where L is the longest diameter and W is the shortest diameter perpendicular to length.

### 2.14. Pharmacokinetics

The rats were weighed and randomly divided into three groups ( $n = 4$ ), and received intravenous injections of different drug-loaded liposomes at a dose of 5 mg/kg PTX and 20 mg/kg LND. After administration, the blood samples were collected at 0.083, 0.25, 0.5, 0.75, 1, 2, 4, 8, 12, 24 h and then centrifuged at 10,000 g for 10 min. The supernatant plasma was obtained and stored at  $-20$  °C until HPLC analysis.

The amount of drug was determined using HPLC as follows. Briefly, 100 µL of plasma was mixed with 80 µL of HCl (1 M) and then vortexed three times. Afterward, 1 mL of ethyl acetate (EA) was added into the solution above and vortexed, followed by centrifugation at 14,000 g for 10 min. The supernatant was

collected, and the supernatant was further added with 1 mL of EA, followed by the same process above. The supernatants were mixed together and evaporated overnight under vacuum. The reconstitution was made by adding 200 µL of the mobile phase consisting of the mixture of acetonitrile:water containing 0.1% trifluoroacetic acid (61:39, v:v), vortexed and centrifuged at 14,000 g for 10 min. The amount of PTX and/or LND was determined using HPLC.

The pharmacokinetic parameters of each formulation was calculated using a non-compartmental model by PK SOLVER, such as the area under the plasma concentration–time curve ( $AUC_{0-\infty}$ ), elimination half-life ( $t_{1/2}$ ), clearance (Cl) and mean residence time (MRT).

### 2.15. Biodistribution

When the tumors reached to 100–200 mm<sup>3</sup>, the MCF-7/MDR tumor-bearing nude mice were intravenously administrated by the DiR-labeled liposomes, DiR-CL and DiR-HA, at DiR dose of 0.2 mg/kg [48]. To further evaluate the tumor targeting capability of HA, the free HA (5 mg/kg) was intravenously injected into the tumor-bearing mice for 1 h, followed by injection of DiR-HA. At the established time point, the mice were euthanized by isofurane and rapidly imaged using a Maestro in vivo fluorescence imaging system (Cri Inc., USA). At 24 h post-administration, the mice were sacrificed. The main normal organs, such as heart, liver, spleen, lung and kidney, as well as the tumor were harvested for *ex vivo* imaging. The region-of-interest (ROI) was circle around the harvested tissues, and the fluorescence intensity of DiR was measured using the Maestro 3 software.

### 2.16. In vivo antitumor efficacy

Once the tumors reached to 100–200 mm<sup>3</sup>, the MCF-7/MDR tumor-bearing nude mice were intravenously administrated by different drug-loaded liposomes, including PTX&LND-CL, PTX&LND-HA and PTX-HA plus LND-HA, at PTX dose of 5 mg/kg and LND dose of 20 mg/kg, and saline as a negative control every other day (four-time injection). Treatment proceeded for 25 days. During the treatment, the tumor sizes and body weights were monitored. After the treatment, the mice were sacrificed and the tumors were harvested for histological analysis using the hematoxylin and eosin (HE) staining.

### 2.17. Statistical analysis

Results were given as mean  $\pm$  standard deviation (S.D.). Statistical significance was tested by two-tailed Student's t-test or one-way ANOVA. Statistical significance was set at \* $P < 0.05$ , high significance was set at \*\* $P < 0.01$ , and extreme significance was set at \*\*\* $P < 0.001$ .

## 3. Results and discussion

### 3.1. Preparation and characterization of liposome

PTX&LND-CL was prepared using the lipid film hydration method, which had a zeta potential of +55 mV due to the introduction of the cationic lipid, HG2C<sub>18</sub> (Table S1). PTX&LND-TPGS-L was obtained by incorporating TPGS into PTX&LND-CL, which had a significantly decreased surface charge of +34 mV by the shielding effect of TPGS. After coating with negatively charged HA via electrostatic interaction, PTX&LND-HA showed a zeta potential of  $-18$  mV. Such a variation in the surface charge of liposome indicated the successful modification of TPGS and HA on the liposome. As shown in Table S1, the average particle sizes of all the

obtained liposomes were less than 120 nm, which are favorable for the EPR effect. The EE of PTX and LND was more than 90% in all the liposome formulations. The TEM examination presented the spherical unilamellar structures and nice dispersity of PTX&LND-CL, PTX&LND-TPGS-L and PTX&LND-HA (Fig. 2A). The particle size was in agreement with that determined using the DLS measurement.

All the liposomes were stable at 4 °C up to one week (Fig. S1). The EE maintained more than 90% in both TPGS and HA liposome up to one week, compared to CL. No significant difference was found on the zeta potential of TPGS-L and CL within one week, while the zeta potential of HA-L showed a slight change from  $-17$  mV to  $-10$  mV. The influence of rat plasma on the EE for 24 h indicated more drug leakage with the CL than either TPGS-L or HA-L (Fig. S2). This could be due to the positive charge of CL which allows it to bind to plasma protein, thereby resulting in the instability of CL and the leakage of drugs.

The release profiles of PTX and LND from different drug-loaded liposomes were evaluated. The encapsulation of PTX and LND by liposomes resulted in the sustained release of both drugs. The release of PTX was about 25% from either PTX&LND-HA or PTX-HA within 48 h, while that of PTX was about 15% from PTX&LND-CL (Fig. 2B). By comparison, approximately 80% of LND was released from all the liposomes within 48 h (Fig. 2C).

### 3.2. Degradation of HA

We investigated the degradation of the HA shell by monitoring the variation in the particle size and zeta potential of HA-coated liposomes after incubation with HAase at different pH values. After incubation with HAase over time, a slight decrease in the particle size of liposome was determined (Fig. 3A). Of note, the change in the zeta potential was more apparent (Fig. 3B). The zeta potentials of all the HA-coated liposomes showed no significant change after incubation with HAase for 3 h at pH 7.4. In sharp contrast, the zeta potential changed from  $-17$  mV to  $+23$  mV after exposure of HAase for 3 h at pH 4.5. These data suggested that the degradation of HA was HAase-mediated and acidic pH-dependent [49]. The HA-coated liposome with the protection of HA that also served as a

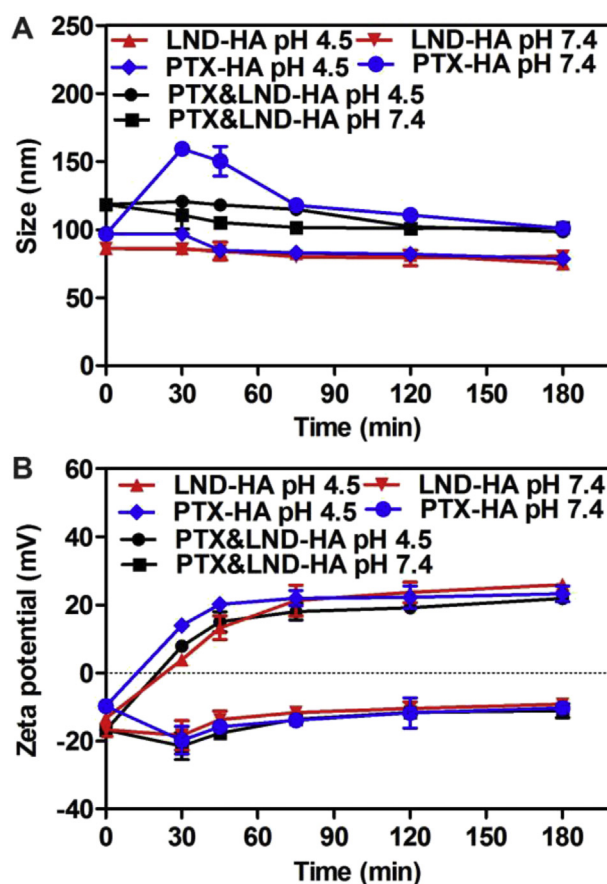


Fig. 3. Change in the particle size (A) and zeta potential (B) of different drug-loaded liposomes after incubation with HAase (1 mg/mL) at different pH (pH 7.4 and 4.5) over time.

targeting ligand accumulated at the tumor site. Following endocytosis, the HA shell was able to be degraded by HAase in the endocytic vesicles, endosomes or lysosomes, which allow the

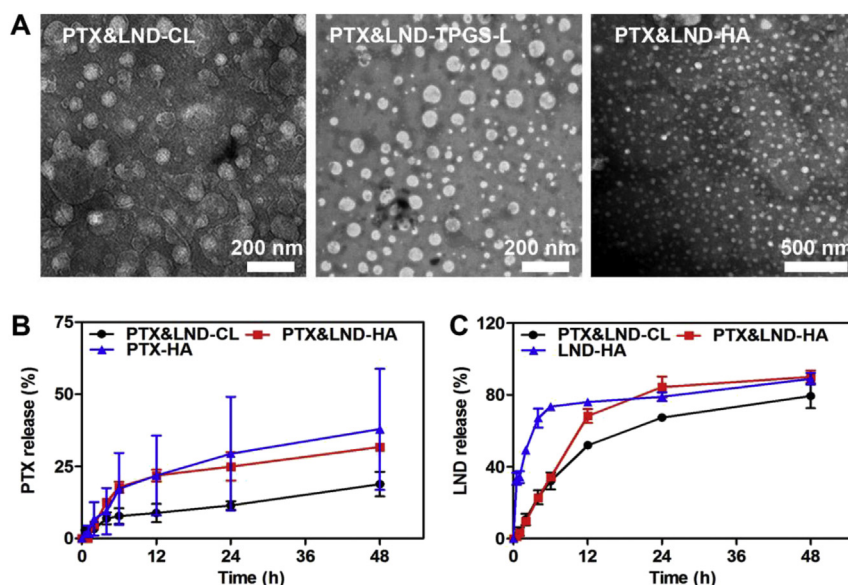


Fig. 2. (A) TEM images of PTX&LND-CL (left), PTX&LND-TPGS-L (middle), PTX&LND-HA (right). (B, C) In vitro release profiles of PTX (B) and LND (C) from different drug-loaded liposomes at pH 7.4 over time.

exposure of TPGS-L for mitochondria targeting.

### 3.3. Cellular uptake and endocytosis pathway

The cellular uptake of different drug-loaded liposomes was estimated on the CD44-overexpressing MCF-7/MDR cells (Fig. S3). All the liposome formulations showed a higher cellular uptake of PTX than Taxol that was even co-delivered with LND, which indicated that Taxol was inevitably subject to the efflux by the over-expressed P-gp in MCF-7/MDR cells. PTX&LND-HA presented the highest cellular uptake of PTX compared to other formulations, including PTX-HA, PTX&LND-CL and cocktail-based co-delivery of PTX-HA with LND-HA. At different concentrations of PTX, the cellular uptake of PTX delivered by PTX&LND-HA was all significantly higher than that delivered by the highly positive charged PTX&LND-CL (Fig. 4A), which indicated that the CD44-mediated endocytosis based on the active targeting effect of HA played an important role on enhanced uptake of liposome compared to the electronic adsorptive endocytosis.

To further demonstrate the interaction between CD44 and HA, we compared the cellular uptake of PTX&LND-HA in the absence and presence of the free HA on different types of cells, such as the CD44-deficient MCF-7 cells and the CD44-overexpressing MCF-7/MDR and A549 cells. The cells were pre-treated with the excessive free HA to block the CD44 receptors on the cell membrane. As shown in Fig. 4B, the cellular uptake of PTX in the presence of HA was comparable to that in the absence of HA on MCF-7 cells, while showed significant decrease on both MCF-7/MDR and A549 cells compared to that without treatment with HA. This result confirmed that PTX&LND-HA was taken up by the cancer cells via the CD44-mediated internalization. Moreover, we incubated PTX&LND-HA with HAase at pH 4.5 for 1 h to degrade the HA shell of liposome, followed by assessing the cellular uptake. As shown in Fig. 4C, the HAase-treated PTX&LND-HA showed a dramatic reduction in the cellular uptake compared to the non-treated one, which further suggested the effect of the HA shell on increasing the intracellular

accumulation of PTX.

Next, we investigated the endocytosis pathways of PTX&LND-HA and PTX&LND-CL on MCF-7/MDR cells (Fig. 4D). Different specific inhibitors were applied to block the corresponding endocytosis pathways. Amiloride that is an inhibitor for macropinocytosis pathway significantly decreased the cellular uptake of PTX&LND-CL, implying PTX&LND-CL was internalized by the cells through the macropinocytosis pathway. In contrast, sucrose, the clathrin-mediated endocytosis pathway inhibitor, remarkably decreased the cellular uptake of PTX&LND-HA compared to other inhibitors, indicating that the modification of TPGS and HA on the liposome affected the endocytosis pathway, which caused PTX&LND-HA to be endocytosed via the clathrin-mediated pathway. Taken together, both of the liposomes were taken up into the endocytic vesicles, endosomes/lysosomes, which were the principal barrier to the intracellular delivery of the liposomes.

### 3.4. Enhanced intracellular accumulation by inhibiting P-gp efflux

The overexpressed P-gp on the cell membrane of the MDR cancer cells has a great effect on the efflux of the anticancer drugs, which results in the low intracellular drug concentration. In view of this, we further focused on evaluating the enhancement of PTX&LND-HA on the intracellular drug accumulation in MCF-7/MDR cells. RH123, a P-gp substrate that is subject to be recognized and secreted by the P-gp, was employed as a model drug [11]. The intracellular accumulation of RH123 delivered by different formulations was observed and quantified using CLSM and flow cytometry, respectively. As shown in Fig. 5A, the free RH123 presented a high fluorescence intensity within MCF-7 cells after incubation for different time, but hardly entered into MCF-7/MDR cells, which indicated a strong P-gp-mediated efflux of RH123 by MCF-7/MDR cells. However, the presence of the free TPGS showed a great capability of promoting the intracellular accumulation of RH123, which confirmed the P-gp inhibiting effect of TPGS for reversal of MDR.

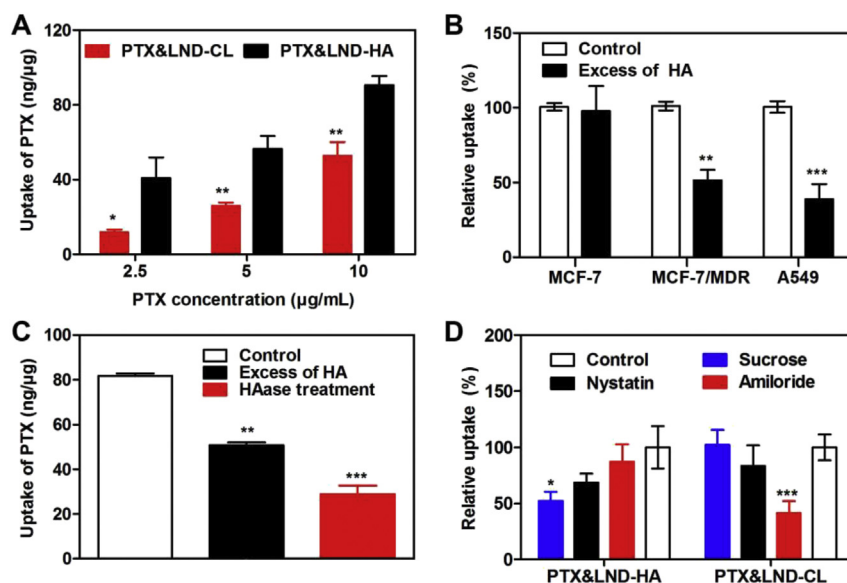


**Fig. 4.** (A) Cellular uptake of PTX&LND-CL and PTX&LND-HA on MCF-7/MDR cells after 4 h of incubation at different PTX concentrations. \* $P < 0.05$ , \*\* $P < 0.01$ , compared to PTX&LND-HA. (B) Relative cellular uptake of PTX&LND-HA on different cancer cells after 4 h of incubation at PTX concentration of 5  $\mu\text{g}/\text{mL}$  in the presence of the free HA compared to that in the absence (control). \*\* $P < 0.01$ , \*\*\* $P < 0.001$ , compared to control. (C) Cellular uptake of PTX&LND-HA on MCF-7/MDR cells after 4 h of incubation at PTX concentration of 5  $\mu\text{g}/\text{mL}$  in the presence of the free HA or after the HAase treatment. \*\* $P < 0.01$ , \*\*\* $P < 0.001$ , compared to control. (D) Relative cellular uptake of PTX&LND-HA on MCF-7/MDR cells after 4 h of incubation at PTX concentration of 5  $\mu\text{g}/\text{mL}$  in the presence of the specific endocytosis inhibitors compared with that in the absence (control). \* $P < 0.05$ , \*\*\* $P < 0.001$ , compared to control.

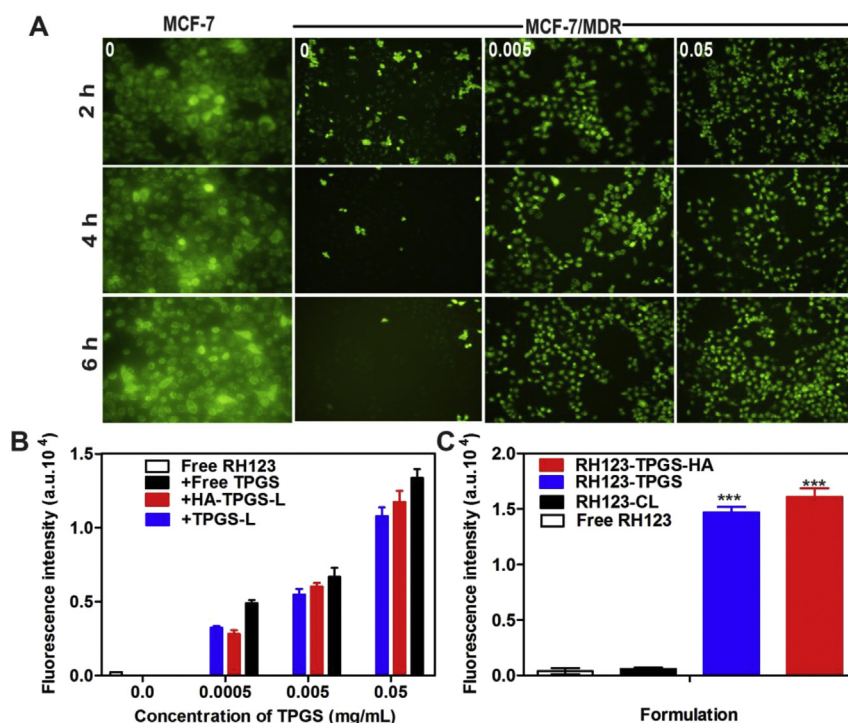


**Fig. 5.** (A) Fluorescence images of MCF-7 and MCF-7/MDR cells after 1 h of incubation with the free RH123 (5  $\mu$ M) in the absence and presence of different concentrations of the free TPGS. Fluorescence images were taken at 400  $\times$  magnification. (B) Fluorescence intensity of MCF-7/MDR cells after 1 h of incubation with the free RH123 (5  $\mu$ M) in the absence and presence of different TPGS formulations at different TPGS concentrations. (C) Fluorescence intensity of MCF-7/MDR cells after 1 h of incubation with different RH123-loaded liposomes at RH123 concentration of 5  $\mu$ M \*\*\* $P$  < 0.001, compared to the free RH123.

Furthermore, the fluorescence intensity of MCF-7/MDR cells after incubation with the free RH123 in the presence of different TPGS-containing formulations was determined using the flow cytometry (Fig. 5B). The TPGS-functionalized liposomes, such as TPGS-L and HA-TPGS-L, were able to evidently enhance the intracellular accumulation of RH123 in MCF-7/MDR cells. This effect was comparable to that of the free TPGS. Additionally, we encapsulated RH123 into different liposomes to acquire RH123-CL, RH123-TPGS-L and RH123-TPGS-HA, and further assessed the cellular uptake of RH123. As shown in Fig. 5C, although RH123 was entrapped in CL, RH123-CL did not show any reinforcement on the intracellular accumulation of RH123 compared to the free RH123. In sharp contrast, both RH123-TPGS and RH123-TPGS-HA had a strong capacity on elevating the cellular uptake of RH123. These results confirmed the MDR reversal effect of TPGS-incorporated liposomes.

### 3.5. Intracellular delivery

The intracellular delivery of different RH123-loaded liposomes was monitored in MCF-7/MDR cells using CLSM. The late endosomes and lysosomes were stained with LysoTracker Red. As shown in Fig. 6A, all RH123-loaded liposomes were internalized into the cells and suffered from the endo-lysosomal entrapment after 3 h of incubation, evidenced by a large area of colocalization between the RH123 signal and the LysoTracker signal shown as yellow fluorescence. As incubation time increased to 6 h, the RH123 signal of the RH123-SPC without the incorporation of HG2C<sub>18</sub> still presented a high colocalization with the endo-lysosomes, which suggested that the conventional liposome hardly penetrated across the endo-lysosomes. Contrarily, the HG2C<sub>18</sub>-containing liposomes including RH123-CL, RH123-TPGS-L and RH123-HA displayed an apparent separation from the endo-lysosomes and a wide distribution within the cells, indicating that HG2C<sub>18</sub> had an essential effect on endo-

lysosome escape based on the high cationic property and the proton sponge effect of the histidine moiety.

Next, we investigated the mitochondria targeting capacity of the liposomes using CLSM (Fig. 6B). The mitochondria in MCF-7/MDR cells were stained with MitoTracker Red. Compared to RH123-SPC and RH123-CL, the TPGS-modified liposomes, RH123-TPGS-L and RH123-HA showed a higher colocalization of the RH123 signal with the MitoTracker signal after 12 h of incubation, which indicated that RH123-TPGS-L and RH123-HA could efficiently deliver the cargoes to the mitochondria due to the mitochondria-targeted characteristics of TPGS. Furthermore, we isolated the mitochondria from the treated cells and quantified the RH123 content in the mitochondria using the flow cytometry. As shown in Fig. 6C, the quantity of RH123 in the mitochondria delivered by either RH123-TPGS-L or RH123-HA was extremely higher than that delivered by both RH123-SPC and RH123-CL, which was in accord with the results obtained from the CLSM observation. Accordingly, the HA-coated and TPGS-functionalized liposomes showed an efficient intracellular delivery, which could migrate from the endo-lysosomes to the cytoplasm and transport to the mitochondria.

### 3.6. Inhibition on intracellular ATP production

After confirming the mitochondria targeting of the liposome, we investigated the influence of PTX&LND-HA on the intracellular ATP production in MCF-7/MDR cells. As shown in Fig. 6D, the cells showed a markedly decreased intracellular ATP level after treatment with all the LND-loaded liposomes, including LND-HA, PTX&LND-HA and PTX-HA plus LND-HA, compared to the untreated cells. However, no significant difference in the ATP level between the untreated cells and the PTX-HA treated cells. Moreover, PTX&LND-HA showed a remarkable effect on inhibiting ATP production compared to PTX-HA. These data suggested that LND

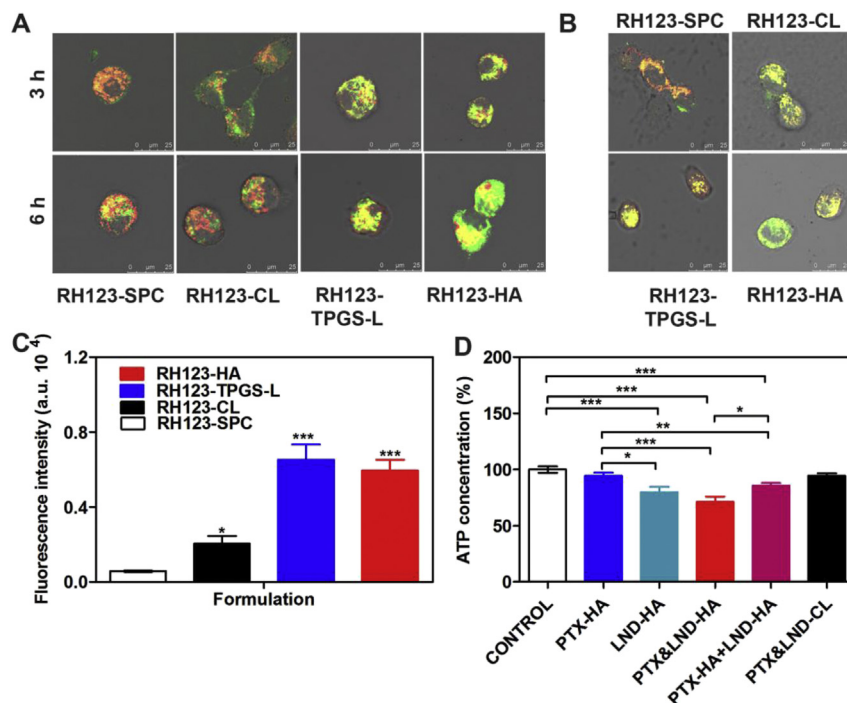


**Fig. 6.** (A) CLSM images of MCF-7/MDR cells after 3 or 6 h of incubation with different RH123-loaded liposomes. The late endosome and lysosome were stained with LysoTracker Red. (B) CLSM images of MCF-7/MDR cells after 12 h of incubation with different RH123-loaded liposomes. The mitochondria were stained with MitoTracker Red. (C) Fluorescence intensity of the isolated mitochondria of MCF-7/MDR cells after 12 h of incubation with different RH123-loaded liposomes. \* $P < 0.05$ , \*\*\* $P < 0.001$ , compared to RH123-SPC. (D) Intracellular ATP level of MCF-7/MDR cells after 8 h of incubation with different drug-loaded liposomes. \* $P < 0.05$ , \*\* $P < 0.01$ , \*\*\* $P < 0.001$ .

was able to interfere with the mitochondrial function to inhibit the intracellular ATP production. In addition, the treatment with PTX&LND-HA resulted in a significant inhibition on the ATP generation compared to the cocktail-based co-delivery of PTX-HA plus LND-HA, due partly to the decreased cellular uptake of LND-HA by the competitive interaction with PTX-HA. Collectively, LND that was efficiently delivered by PTX&LND-HA acted on the mitochondria and suppressed the ATP production, which could further not only inhibit the P-gp efflux by the synergistic effect with TPGS, but also sensitize the cancer cells to PTX for elevated induction of apoptosis and cytotoxicity.

### 3.7. Cell apoptosis and cytotoxicity

The apoptosis-inducing effect of PTX&LND-HA was first evaluated using the Hoechst and PI double staining. As shown in Fig. 7A, the nuclei of the untreated cells showed homogeneous fluorescence with no evidence of segmentation and fragmentation after Hoechst staining, while the cell nuclei became severely fragmented when the cells were treated with different drug formulations for 12 h, suggesting that the nuclei were segmented into dense nuclear parts and further distributed into apoptotic bodies. The PI staining for late apoptotic cells only showed the homogeneous fluorescence, in line with the cell death process.

Furthermore, the annexin V-FITC/PI apoptosis detection kit was used to quantitatively determine the apoptotic effects. As shown in Fig. 7B, PTX&LND-HA had the strongest apoptosis-inducing capacity compared to other drug formulations. The MCF-7/MDR cells after treatment with PTX&LND-HA for 12 h had the total apoptotic ratio of 22.3%, much higher than 6.5% of Taxol co-delivered with the free LND, 11.2% of PTX&LND-CL and 17.4% of PTX-HA co-delivered with LND-HA.

The cytotoxicity of PTX&LND-HA was estimated against MCF-7/

MDR cells using the MTT assay (Fig. 7C). As expected, PTX&LND-HA showed the significantly higher cytotoxicity toward MCF-7/MDR cells than other drug formulations after 48 h of incubation. The half maximal inhibitory concentration (IC<sub>50</sub>) of PTX&LND-HA was about 0.06  $\mu\text{g}/\text{mL}$  (Table S2), extremely lower than 0.15  $\mu\text{g}/\text{mL}$  of PTX-HA, 9.51  $\mu\text{g}/\text{mL}$  of PTX&LND-CL, 1.48  $\mu\text{g}/\text{mL}$  of Taxol co-delivered with the free LND, and 0.12  $\mu\text{g}/\text{mL}$  of PTX-HA co-delivered with LND-HA. Additionally, the mixture of Cremophor EL and ethanol without PTX displayed noticeable cytotoxicity, compared to TPGS-HA-L, the blank vehicle of PTX&LND-HA (Fig. 7D).

Accordingly, it is confirmed that the combination of increased cellular uptake by the active targeting effect of HA, efficient intracellular delivery, P-gp inhibition by TPGS and LND, and LND-mediated cell sensitization to cytotoxic agent resulted in a remarkable enhancement of PTX on inducing the apoptosis and cytotoxicity by PTX&LND-HA.

### 3.8. Pharmacokinetics and biodistribution

The pharmacokinetics of different drug-loaded liposomes were assessed after intravenous injection into the rats. The plasma concentration–time curves were shown in Fig. 8A. The relative pharmacokinetic parameters were calculated to quantitatively evaluate the pharmacokinetic property (Table S3). PTX&LND-HA rendered improved blood persistence of both PTX and LND compared to PTX&LND-CL, substantiated by the higher AUC, longer  $t_{1/2}$  and MRT, and lower Cl, which allowed enhanced tumor targetability and therapeutic index in vivo.

The biodistribution of the liposome after intravenous injection into the MCF-7/MDR tumor-bearing mice was monitored using the in vivo imaging technique. The liposomes, CL and TPGS-HA-L, were labeled with the lipophilic dye, DiR. As shown in Fig. 8B, DiR-HA efficiently accumulated at the tumor site at just 1 h post

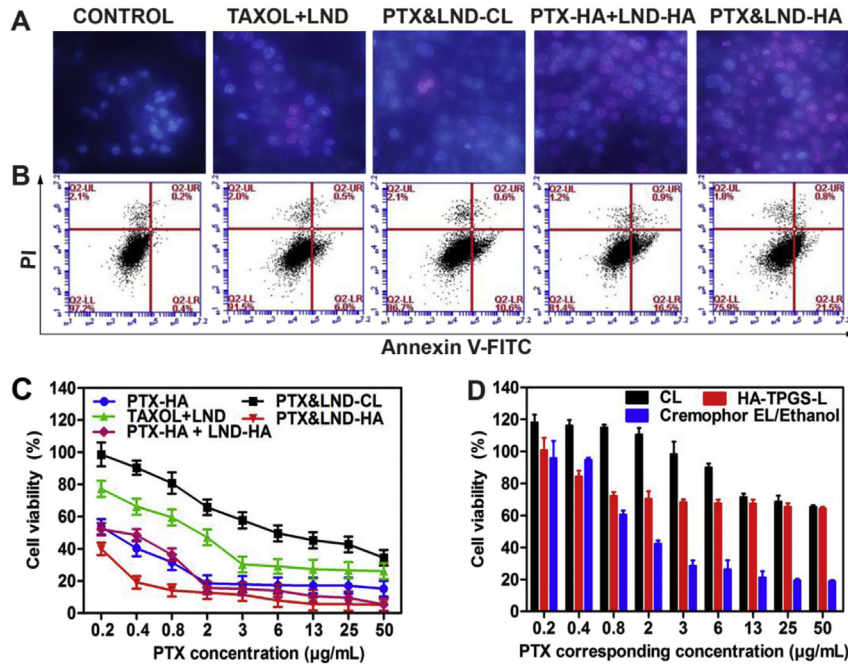


**Fig. 7.** (A) Fluorescence images of MCF-7/MDR cells after 12 h of incubation with different drug formulations. The nuclei were stained with Hoechst and PI. Fluorescence images were taken at 400 × magnification. (B) Apoptosis of MCF-7/MDR cells induced by different drug formulations after 12 h of incubation determined using the Annexin V-FITC/PI staining. In each panel, the lower-left, lower-right and upper-right quadrants represent the population of the viable, early apoptotic and late apoptotic cells, respectively. (C) In vitro cytotoxicity of different drug formulations against MCF-7/MDR cells after 48 h of incubation. (D) In vitro cytotoxicity of different blank vehicles without drugs against MCF-7/MDR cells after 48 h of incubation.

injection, and the DiR signal maintained up to 24 h. By comparison, DiR-CL presented an inferior tumor targeting capacity. To further assess the active targeting effect of the HA shell of DiR-HA, the tumor-bearing mice was pre-injected with the high concentration

of the free HA solution for competitively blocking the CD44 receptors on the tumor cells, followed by injection with DiR-HA. The DiR signal apparently decreased at the tumor region as expected. For *ex vivo* imaging, the DiR signal of DiR-HA in the harvested tumor

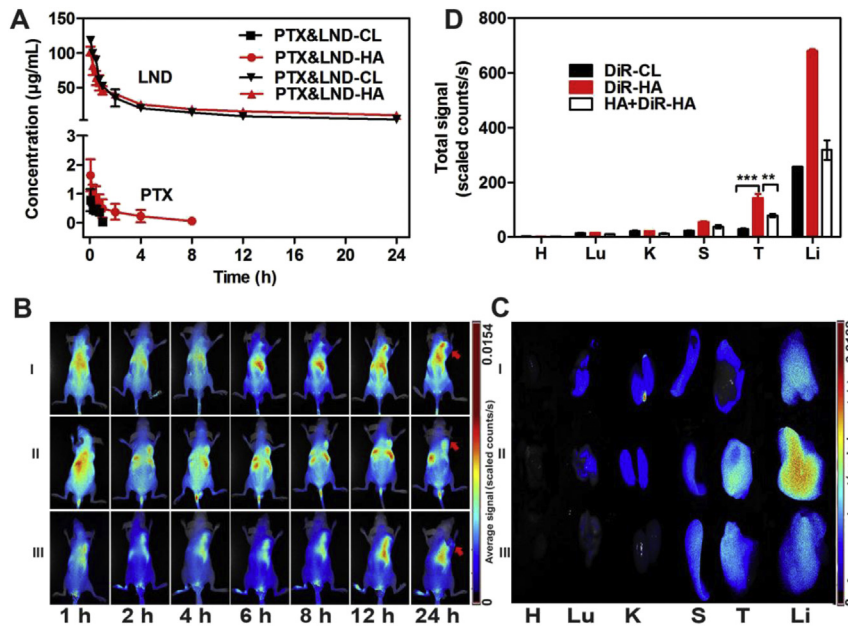


**Fig. 8.** (A) Plasma concentration–time curve of PTX (lower) and LND (upper) in the rats after intravenous injection of PTX&LND-HA and PTX&LND-CL at PTX dose of 5 mg/kg and LND dose of 20 mg/kg. (B) In vivo fluorescence imaging of the MCF-7/MDR tumor-bearing nude mice after intravenous injection with DiR-CL (I), DiR-HA (II) and DiR-HA with pre-injection of the free HA (5 mg/kg) for 1 h (III) at DiR dose of 0.2 mg/kg over time. The red arrow indicates the tumor region. (C) Ex vivo fluorescence images of different tissues harvested from the mice at 24 h post-injection, including heart (H), lung (Lu), kidney (K), spleen (S), tumor (T) and liver (Li). (D) Fluorescence intensity of the DiR signals in different tissues harvested from the mice at 24 h post-injection. \*\* $P < 0.01$ , \*\*\* $P < 0.001$ . (For interpretation of the references to colour in this figure legend, the reader is referred to the web version of this article.)

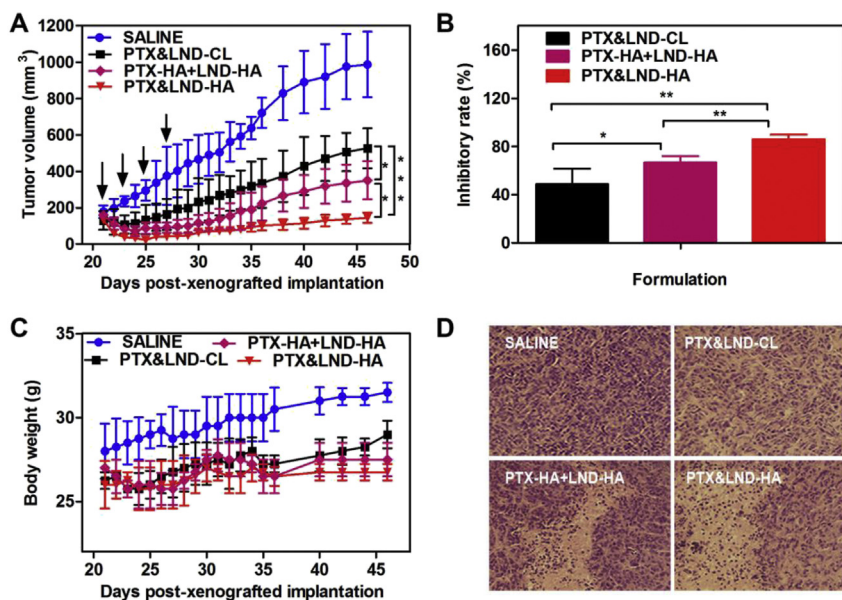


**Fig. 9.** (A) Changes in the tumor volume of the MCF-7/MDR tumor-bearing nude mice receiving intravenous injection of PTX&LND-CL, PTX&LND-HA and PTX-HA plus LND-HA at PTX dose of 5 mg/kg and LND dose of 20 mg/kg, and saline. \* $P < 0.05$ , \*\*\* $P < 0.001$ . (B) Tumor volume inhibitory rate after treatment with PTX&LND-CL, PTX&LND-HA and PTX-HA plus LND-HA. \* $P < 0.05$ , \*\* $P < 0.01$ . (C) Changes in the body weight of the mice during treatment. (D) Representative images of the HE-stained tumor sections after treatment with PTX&LND-CL, PTX&LND-HA and PTX-HA plus LND-HA. The images were taken at  $400 \times$  magnification.

of the mice after injection for 24 h was noticeably higher than that of DiR-CL (Fig. 8C), although the strong DiR signal was detected in the liver due to the preferential cellular uptake of HA by the liver sinusoidal endothelial cells [50–52]. The pre-injection with the high concentration of free HA resulted in decreased liver accumulation of DiR-HA by the competitive blocking effect of HA on the cellular uptake of DiR-HA in the liver. The quantitative ROI analysis further confirmed the superior tumor target ability of DiR-HA (Fig. 8D). The fluorescence intensity of the DiR signal of DiR-HA was about 4.9-fold and 1.8-fold that of DiR-CL and DiR-HA plus HA, respectively. These data validated that DiR-HA had a high tumor-targeting efficiency through a combination of the EPR-based passive targeting and HA-mediated active targeting effects.

### 3.9. In vivo antitumor efficacy

The in vivo antitumor efficacy of different drug formulations was evaluated on the MCF-7/MDR tumor-bearing mice. As shown in Fig. 9A, all the PTX and LND co-loaded liposomes presented great effects on inhibiting the tumor growth after successive intravenous injection into the tumor-bearing mice. Cocktail-based co-delivery of PTX-HA and LND-HA had a stronger tumor inhibition capacity than PTX&LND-CL, which was mainly attributed to the improved pharmacokinetic behavior and tumor-targeting capability of the liposomes functionalized by HA and TPGS. Note that a significant difference was observed in the inhibition of the tumor growth between PTX&LND-HA and PTX-HA plus LND-HA, suggesting that the co-encapsulation of PTX and LND in one nanocarrier could optimize the pharmacokinetic property and biodistribution behavior between two drugs for enhanced synergistic antitumor activity [53,54]. The inhibitory rate of PTX&LND-HA was higher than 85% compared to 65% of PTX-HA plus LND-HA (Fig. 9B). The images of the tumor harvested from the mice visually showed the greatest tumor shrinkage after treatment with PTX&LND-HA (Fig. S4). No remarkable change in body weight was observed during the treatment with PTX&LND-HA (Fig. 9C). The histological analysis of the tumor that was harvested from the mice after

treatment of PTX&LND-HA using the HE staining showed a greater remission of the tumor cells, compared to that after treatment with other formulations (Fig. 9D), which further evidenced the superior therapeutic efficacy of PTX&LND-HA.

## 4. Conclusion

In summary, we have developed a co-delivery strategy of PTX and LND using a TPGS and HA dual-functionalized liposome to overcome MDR for enhanced cancer therapy. The liposome rendered a high drug accumulation in the tumor tissue, maintained a high intracellular drug concentration within the tumor cells, and displayed an efficient intracellular delivery, thereby yielding the reversal of MDR and elevated cancer treatment. This strategy provides a great potential for exploration of novel anticancer DDSs for treating the MDR cancer.

## Acknowledgment

This work was supported by the National Natural Science Foundation of China (81273468, 81473153), National Basic Research Program of China (2015CB755500), Natural Science Foundation of Jiangsu Province of China (BK20140672), Fundamental Research Funds for the Central Universities of China (0201000144), State Key Laboratory of Natural Medicines at China Pharmaceutical University (CPU) (SKLNMZCX201401) and 111 Project from the Ministry of Education of China and the State Administration of Foreign Expert Affairs of China (No. 111-2-07). This work was also supported by the Jiangsu Specially-Appointed Professors Program, the CPU High-Level Talent Program and the start-up package from CPU to R.M.

## Appendix A. Supplementary data

Supplementary data related to this article can be found at <http://dx.doi.org/10.1016/j.biomaterials.2015.09.022>.

## References

- [1] C. Holohan, S. Van Schaeybroeck, D.B. Longley, P.G. Johnston, Cancer drug resistance: an evolving paradigm, *Nat. Rev. Cancer* 13 (2013) 714–726.
- [2] K. Nooter, G. Stoter, Molecular mechanisms of multidrug resistance in cancer chemotherapy, *Pathol. Res. Pract.* 192 (1996) 768–780.
- [3] A. Stege, A. Priesch, C. Nieth, H. Lage, Stable and complete overcoming of MDR1/P-glycoprotein-mediated multidrug resistance in human gastric carcinoma cells by RNA interference, *Cancer Gene Ther.* 11 (2004) 699–706.
- [4] B.C. Baguley, Multiple drug resistance mechanisms in cancer, *Mol. Biotechnol.* 46 (2010) 308–316.
- [5] K.W. Scotto, Transcriptional regulation of ABC drug transporters, *Oncogene* 22 (2003) 7496–7511.
- [6] R. Callaghan, F. Luk, M. Bebawy, Inhibition of the multidrug resistance P-glycoprotein: time for a change of strategy? *Drug Metab. Dispos.* 42 (2014) 623–631.
- [7] A.S. Prakash, Selecting surfactants for the maximum inhibition of the activity of the multidrug resistance efflux pump transporter, P-glycoprotein: conceptual development, *J. Excip. Food Chem.* 1 (2010) 51–59.
- [8] M. Werle, Natural and synthetic polymers as inhibitors of drug efflux pumps, *Pharm. Res.* 25 (2008) 500–511.
- [9] J.M. Dintaman, J.A. Silverman, Inhibition of P-glycoprotein by D-alpha-tocopheryl polyethylene glycol 1000 succinate (TPGS), *Pharm. Res.* 16 (1999) 1550–1556.
- [10] E.V. Batrakova, A.V. Kabanov, Pluronic block copolymers: evolution of drug delivery concept from inert nanocarriers to biological response modifiers, *J. Control Release* 130 (2008) 98–106.
- [11] R. Mo, X. Jin, N. Li, C. Ju, M. Sun, C. Zhang, et al., The mechanism of enhancement on oral absorption of paclitaxel by N-octyl-O-sulfate chitosan micelles, *Biomaterials* 32 (2011) 4609–4620.
- [12] X. Jin, R. Mo, Y. Ding, W. Zheng, C. Zhang, Paclitaxel-loaded N-octyl-O-sulfate chitosan micelles for superior cancer therapeutic efficacy and overcoming drug resistance, *Mol. Pharm.* 11 (2014) 145–157.
- [13] E.M. Kemper, A.E. van Zandbergen, C. Cleypool, H.A. Mos, W. Boogerd, J.H. Beijnen, et al., Increased penetration of paclitaxel into the brain by inhibition of P-glycoprotein, *Clin. Cancer Res.* 9 (2003) 2849–2855.
- [14] S. Shukla, S. Ohnuma, S.V. Ambudkar, Improving cancer chemotherapy with modulators of ABC drug transporters, *Curr. Drug Targets* 12 (2011) 621–630.
- [15] H. Thomas, H.M. Coley, Overcoming multidrug resistance in cancer: an update on the clinical strategy of inhibiting P-glycoprotein, *Cancer Control* 10 (2003) 159–165.
- [16] V.K. Yellepeddi, K.K. Vangara, A. Kumar, S. Palakurthi, Comparative evaluation of small-molecule chemosensitizers in reversal of cisplatin resistance in ovarian cancer cells, *Anticancer Res.* 32 (2012) 3651–3658.
- [17] L. Wu, J. Xu, W. Yuan, B. Wu, H. Wang, G. Liu, et al., The reversal effects of 3-bromopyruvate on multidrug resistance in vitro and in vivo derived from human breast MCF-7/ADR cells, *PLoS One* 9 (2014) e112132.
- [18] L. Ravagnan, I. Marzo, P. Costantini, S.A. Susin, N. Zamzami, P.X. Petit, et al., Loniidamine triggers apoptosis via a direct, Bcl-2-inhibited effect on the mitochondrial permeability transition pore, *Oncogene* 18 (1999) 2537–2546.
- [19] H.I. Robins, W.L. Longo, R.K. Lagoni, A.J. Neville, A. Hugander, C.L. Schmitt, et al., Phase I trial of lonidamine with whole body hyperthermia in advanced cancer, *Cancer Res.* 48 (1988) 6587–6592.
- [20] R. Rosso, G. Gardin, P. Pronzato, A. Camoriano, L. Merlini, C. Naso, et al., The role of lonidamine in the treatment of breast cancer patients, *Ann. N. Y. Acad. Sci.* 698 (1993) 349–356.
- [21] S. Di Cosimo, G. Ferretti, P. Papaldo, P. Carlini, A. Fabi, F. Cognetti, Lonidamine: efficacy and safety in clinical trials for the treatment of solid tumors, *Drugs Today (Barc)* 39 (2003) 157–174.
- [22] A.R. Kirtane, S.M. Kalscheuer, J. Panyam, Exploiting nanotechnology to overcome tumor drug resistance: challenges and opportunities, *Adv. Drug Deliv. Rev.* 65 (2013) 1731–1747.
- [23] P. Kreuzaler, C.J. Watson, Killing a cancer: what are the alternatives? *Nat. Rev. Cancer* 12 (2012) 411–424.
- [24] Y. Zhang, H.F. Chan, K.W. Leong, Advanced materials and processing for drug delivery: the past and the future, *Adv. Drug Deliv. Rev.* 65 (2013) 104–120.
- [25] X. Dong, R.J. Mumper, Nanomedicinal strategies to treat multidrug-resistant tumors: current progress, *Nanomedicine (Lond)* 5 (2010) 597–615.
- [26] A. Schroeder, D.A. Heller, M.M. Winslow, J.E. Dahlman, G.W. Pratt, R. Langer, et al., Treating metastatic cancer with nanotechnology, *Nat. Rev. Cancer* 12 (2012) 39–50.
- [27] R.A. Petros, J.M. DeSimone, Strategies in the design of nanoparticles for therapeutic applications, *Nat. Rev. Drug Discov.* 9 (2010) 615–627.
- [28] B.D. Grant, J.G. Donaldson, Pathways and mechanisms of endocytic recycling, *Nat. Rev. Mol. Cell Biol.* 10 (2009) 597–608.
- [29] V.P. Torchilin, Recent advances with liposomes as pharmaceutical carriers, *Nat. Rev. Drug Discov.* 4 (2005) 145–160.
- [30] R. Mo, T. Jiang, Z. Gu, Recent progress in multidrug delivery to cancer cells by liposomes, *Nanomedicine (Lond)* 9 (2014) 1117–1120.
- [31] M.S. Muthu, S.A. Kulkarni, A. Raju, S.S. Feng, Theranostic liposomes of TPGS coating for targeted co-delivery of docetaxel and quantum dots, *Biomaterials* 33 (2012) 3494–3501.
- [32] N. Li, C.X. Zhang, X.X. Wang, L. Zhang, X. Ma, J. Zhou, et al., Development of targeting lonidamine liposomes that circumvent drug-resistant cancer by acting on mitochondrial signaling pathways, *Biomaterials* 34 (2013) 3366–3380.
- [33] Y. Obata, D. Suzuki, S. Takeoka, Evaluation of cationic assemblies constructed with amino acid based lipids for plasmid DNA delivery, *Bioconjug Chem.* 19 (2008) 1055–1063.
- [34] J. Neuzil, L.F. Dong, L. Ramanathapuram, T. Hahn, M. Chladova, X.F. Wang, et al., Vitamin E analogues as a novel group of mitocans: anti-cancer agents that act by targeting mitochondria, *Mol. Asp. Med.* 28 (2007) 607–645.
- [35] T. Jiang, R. Mo, A. Bellotti, J. Zhou, Z. Gu, Gel–liposome-mediated co-delivery of anticancer membrane-associated proteins and small-molecule drugs for enhanced therapeutic efficacy, *Adv. Funct. Mater.* 24 (2014) 2295–2304.
- [36] P. Bertrand, N. Girard, C. Duval, J. d'Anjou, C. Chauzy, J.F. Menard, et al., Increased hyaluronidase levels in breast tumor metastases, *Int. J. Cancer* 73 (1997) 327–331.
- [37] T. Jiang, Z. Zhang, Y. Zhang, H. Lv, J. Zhou, C. Li, et al., Dual-functional liposomes based on pH-responsive cell-penetrating peptide and hyaluronic acid for tumor-targeted anticancer drug delivery, *Biomaterials* 33 (2012) 9246–9258.
- [38] R. Mo, Q. Sun, J. Xue, N. Li, W. Li, C. Zhang, et al., Multistage pH-responsive liposomes for mitochondrial-targeted anticancer drug delivery, *Adv. Mater.* 24 (2012) 3659–3665.
- [39] A.K. Varkouhi, M. Scholte, G. Storm, H.J. Haisma, Endosomal escape pathways for delivery of biologicals, *J. Control Release* 151 (2011) 220–228.
- [40] L. Milane, Z. Duan, M. Amiji, Development of EGFR-targeted polymer blend nanocarriers for combination paclitaxel/lonidamine delivery to treat multidrug resistance in human breast and ovarian tumor cells, *Mol. Pharm.* 8 (2011) 185–203.
- [41] B.A. Teicher, T.S. Herman, S.A. Holden, R. Epelbaum, S.D. Liu, E. Frei 3rd, Lonidamine as a modulator of alkylating agent activity in vitro and in vivo, *Cancer Res.* 51 (1991) 780–784.
- [42] R. Mo, Q. Sun, N. Li, C. Zhang, Intracellular delivery and antitumor effects of pH-sensitive liposomes based on zwitterionic oligopeptide lipids, *Biomaterials* 34 (2013) 2773–2786.
- [43] R.U. Takahashi, F. Takeshita, K. Honma, M. Ono, K. Kato, T. Ochiya, Ribophorin II regulates breast tumor initiation and metastasis through the functional suppression of GSK3 $\beta$ , *Sci. Rep.* 3 (2013) 2474.
- [44] S. Akunuru, Q. James Zhai, Y. Zheng, Non-small cell lung cancer stem/progenitor cells are enriched in multiple distinct phenotypic subpopulations and exhibit plasticity, *Cell Death Dis.* 3 (2012) e352.
- [45] G. Chang, J. Wang, H. Zhang, Y. Zhang, C. Wang, H. Xu, et al., CD44 targets Na<sup>+</sup>/H<sup>+</sup> exchanger 1 to mediate MDA-MB-231 cells' metastasis via the regulation of ERK1/2, *Br. J. Cancer* 110 (2014) 916–927.
- [46] C. Frezza, S. Cipolat, L. Scorrano, Organelle isolation: functional mitochondria from mouse liver, muscle and cultured fibroblasts, *Nat. Protoc.* 2 (2007) 287–295.
- [47] S.N. Syed Abdul Rahman, N. Abdul Wahab, S.N. Abd Malek, In vitro morphological assessment of apoptosis induced by antiproliferative constituents from the rhizomes of curcuma zedoaria, *Evid. Based Complement. Altern. Med.* 2013 (2013) 257108.
- [48] V. Krishnan, X. Xu, S.P. Barwe, X. Yang, K. Czymmek, S.A. Waldman, et al., Dexamethasone-loaded block copolymer nanoparticles induce leukemia cell death and enhances therapeutic efficacy: a novel application in pediatric nanomedicine, *Mol. Pharm.* 10 (2013) 2199–2210.
- [49] R. Mo, T. Jiang, R. DiSanto, W. Tai, Z. Gu, ATP-triggered anticancer drug delivery, *Nat. Commun.* 5 (2014) 3364.
- [50] K.Y. Choi, K.H. Min, H.Y. Yoon, K. Kim, J.H. Park, I.C. Kwon, et al., PEGylation of hyaluronic acid nanoparticles improves tumor targetability in vivo, *Biomaterials* 32 (2011) 1880–1889.
- [51] M.S. Pandey, E.N. Harris, J.A. Weigel, P.H. Weigel, The cytoplasmic domain of the hyaluronan receptor for endocytosis (HARE) contains multiple endocytic motifs targeting coated pit-mediated internalization, *J. Biol. Chem.* 283 (2008) 21453–21461.
- [52] Q. Sun, Z. Kang, L. Xue, Y. Shang, Z. Su, H. Sun, et al., A collaborative assembly strategy for tumor-targeted siRNA delivery, *J. Am. Chem. Soc.* 137 (2015) 6000–6010.
- [53] L.D. Mayer, T.O. Harasym, P.G. Tardi, N.L. Harasym, C.R. Shew, S.A. Johnstone, et al., Ratiometric dosing of anticancer drug combinations: controlling drug ratios after systemic administration regulates therapeutic activity in tumor-bearing mice, *Mol. Cancer Ther.* 5 (2006) 1854–1863.
- [54] G. Batist, K.A. Gelmon, K.N. Chi, W.H. Miller Jr., S.K. Chia, L.D. Mayer, et al., Safety, pharmacokinetics, and efficacy of CPX-1 liposome injection in patients with advanced solid tumors, *Clin. Cancer Res.* 15 (2009) 692–700.